Environmental Science & Technology

pubs.acs.org/est

Article

Ionic Strength Effect Triggers Brown Carbon Formation through Heterogeneous Ozone Processing of Ortho-Vanillin

Yiqun Wang, Majda Mekic, Pan Li, Huifan Deng, Shiyang Liu, Bin Jiang, Biao Jin, Davide Vione, and Sasho Gligorovski*

Cite This: *Environ. Sci. Technol.* 2021, 55, 4553−4564

Read Online

ACCESS | Metrics & More | Article Recommendations | Supporting Information

ABSTRACT: Methoxyphenols are an important class of compounds emerging from biomass combustion, and their reactions with ozone can generate secondary organic aerosols in the atmosphere. Here, we use a vertical wetted wall flow tube reactor to evaluate the effect of ionic strength on the heterogeneous reaction of gas-phase ozone (O_3) with a liquid film of *o*-vanillin (*o*-VL) (2-hydroxy-3-methoxybenzaldehyde), as a proxy for methoxyphenols. Typical for moderately acidic aerosols, at fixed pH = 5.6, the uptake coefficients (γ) of O_3 on *o*-VL ([*o*-VL] = 1×10^{-5} mol L^{-1}) increase from $\gamma = (1.9 \pm 0.1) \times 10^{-7}$ in the absence of Na_2SO_4 to $\gamma = (6.8 \pm 0.3) \times 10^{-7}$ at I = 0.2 mol L^{-1}, and then, it decreases again. The addition of NO_3^- ions only slightly decreases the uptakes of O_3. Ultrahigh-resolution electrospray ionization Fourier transform ion cyclotron resonance mass spectrometry (FT-ICR MS) reveals that the formation of multicore aromatic compounds is favored upon heterogeneous O_3 reaction with *o*-VL, in the presence of SO_4^{2-} and NO_3^- ions. The addition of NO_3^- ions favors the formation of nitrooxy ($-ONO_2$) or oxygenated nitrooxy group of organonitrates, which are components of brown carbon that can affect both climate and air quality.

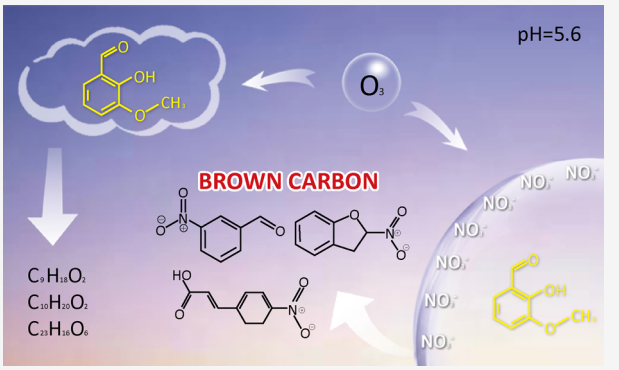

1. INTRODUCTION

Wood combustion and biomass burning (BB) generate significant amounts of methoxyphenols arising from the pyrolysis of lignin.[1,2] The photochemically induced transformation of polycyclic aromatic hydrocarbons, which are also emitted by BB, is an important additional source of methoxyphenols.[3] The methoxyphenols represented ca. 45% of the total aerosol mass produced by wood-burning smoke.[4] Therefore, methoxyphenols were used in many studies as relatively stable tracers of wood smoke to determine its contribution to aerosols. Simpson et al. (2005)[1] detected methoxyphenols in the ng m^{-3} order, in ambient aerosol samples, with the most abundant compounds being vanillin, syringaldehyde, coniferylaldehyde, and sinapylaldehyde. For this reason, in this work, we have chosen 2-hydroxy-3-methoxybenzaldehyde (ortho-vanillin, *o*-VL) as a model compound of methoxyphenols.[5,6] The Henry's law coefficient of vanillin is relatively high (4.56×10^5 M atm^{-1} at 298 K),[7] implying that aqueous-phase photochemical oxidation reactions represent an important *o*-VL transformation pathway, which could potentially initiate secondary organic aerosol (SOA) formation in the atmosphere.[8−10]

The photodegradation and the reactions of methoxyphenols with atmospherically relevant oxidants, such as ozone (O_3), nitrate radicals (NO_3), chlorine atoms (Cl), and hydroxyl radicals (OH) have been extensively studied in the past.[11−17] A study of photooxidation of vanillin in the presence of nitrite (NO_2^-) at different pH values showed that nitrophenols are the major reaction products.[18]

The ionic strength (I) in cloud droplets varies between 7.5×10^{-5} and 7.5×10^{-4} mol L^{-1},[19] while in marine aerosols, it goes up to 6 mol L^{-1}.[20] Moreover, aerosol particles in the urban atmosphere can reach I = 18.6 mol L^{-1},[19] and haze particles can reach ionic strength values of up to 43 mol L^{-1}.[21]

Therefore, the rates of the photochemical degradation of organic constituents in clouds can be quite different from those in aerosol deliquescent particles.[22] However, our understanding of the ionic-strength effect on the photochemical degradation of organic compounds in aerosols is still in its infancy, compared to that for photooxidation in clouds. Recently, the photochemical degradation of two methoxyphenols, syringaldehyde and acetosyringone, has been investigated at low ionic strength values that are typical for cloud

Received: February 6, 2021
Revised: March 13, 2021
Accepted: March 17, 2021
Published: March 30, 2021

https://doi.org/10.1021/acs.est.1c00874
Environ. Sci. Technol. 2021, 55, 4553−4564

droplets.[23] The rates of degradation of syringaldehyde and acetosyringone were 1.5 and 3.5 times faster, respectively, in the presence of nitrate (NO_3^-) ions ($I = 2.3 \times 10^{-5}$ mol L^{-1}) than in sulfate (SO_4^{2-}) solutions ($I = 2 \times 10^{-4}$ mol L^{-1}).[23]

At pH 3, typical for acidic aerosol particles, a sharp increase has been observed for the uptake coefficients of O_3 on aqueous acetosyringone (ACS) ([ACS] = 1×10^{-6} mol L^{-1}), from $\gamma = (1.39 \pm 0.38) \times 10^{-7}$ in the absence of salt to $\gamma = (1.17 \pm 0.01) \times 10^{-6}$ at $I = 0.9$ mol L^{-1}, adjusted with Na_2SO_4.[24]

In this study, we use a vertical wetted wall flow tube (VWWFT) reactor to investigate the influence of sulfate and nitrate ions on the heterogeneous reactions of O_3 with *o*-VL, in the dark and under light irradiation (320 nm< λ < 400 nm), at pH 5.6 that corresponds to moderately acidic aerosol particles. Indeed, there are a number of recent studies showing that the pH values of aerosol particles under hazy and foggy conditions in China are higher compared to pH values of aerosols in Europe and the USA.[21,25−27] The combined experimental and field results provided convincing evidence that the pH value of aerosol particles is sufficiently high to promote SO_2 oxidation by NO_2 under polluted conditions in China.[26] A pH range of 4.7−6.9 was estimated in winter fog in Beijing.[27] Cheng et al. (2016)[21] have shown that the aqueous S(IV) concentrations increase by 2 orders of magnitude through S(IV)−NO_2 reaction when the solution pH increases from 4 to 5.4−6.2. Shi et al. (2017)[25] defined a moderately polluted region (3 < pH < 6), where secondary nitrate and sulfate were the most abundant water soluble (WS) ions.[25] The oligomeric species formed during the heterogeneous reactions of O_3 with *o*-VL were evaluated by ultrahigh-resolution electrospray ionization Fourier transform ion cyclotron resonance mass spectrometry (FT-ICR MS). The formation of oxygenated aliphatic CHO compounds and multicore aromatics were observed upon heterogeneous reaction of gas-phase ozone with *o*-VL in a dilute aqueous phase corresponding to cloud droplets, while the addition of NO_3^- ions typical of aerosol deliquescent particles favored the formation of organonitrates, which represent typical brown carbon components.

2. EXPERIMENTAL SECTION

2.1. Experimental Set-Up. The heterogeneous reaction between gas-phase O_3 and a 1mm-thin aqueous layer containing either *o*-VL or a mixture of *o*-VL with SO_4^{2-} or NO_3^- at different concentrations was investigated using a VWWFT connected to an O_3 analyzer. The details of this experimental set-up have been provided in our previous papers.[24,28] The flow tube is 80 cm long, with an internal diameter (d) = 0.9 cm. Gaseous ozone was generated by an ozone generator (UVP, LLC Upland). The generated ozone was implemented into the vertically aligned flow tube by a movable glass injector,[24,28] and the ozone concentrations were measured online at the exit of the flow tube by an ozone analyzer (Thermo Scientific model 49i, USA).

A thermostated bath (Lauda, RC Germany) was used to maintain a constant temperature in the flow tube (296 (±0.02) K). Aqueous solutions of *o*-VL ([*o*-VL] = 1×10^{-5} mol L^{-1}) (Sigma-Aldrich, 98.5%) or mixtures of *o*-VL with Na_2SO_4 (Sigma-Aldrich, ≥99.0%) or $NaNO_3$ (Sigma-Aldrich, ≥99.0%) were prepared with ultrapure water (Sartorius 18 MΩ, H_2O-MM-UV-T, Germany). The experiments related to the dependence of the uptake coefficients on the *o*-VL concentrations (Figure 1, see below) were performed at the following concentrations of *o*-VL: 1×10^{-5}, 3×10^{-5}, 4.5×10^{-5}, and 1×10^{-4} mol L^{-1}. The pH values of the *o*-VL solutions were measured by a pH meter (Mettler Toledo). Adding different concentrations of Na_2SO_4 to an aqueous solution containing *o*-VL (1×10^{-5} mol L^{-1}) alters its pH (see Table S2). For the rest of the experiments, to simulate the pH of clouds and moderately acidic particles, pH was adjusted to 5.6 by drop-wise addition of a prepared 1 M solution of HCl. Then, the prepared solution was continuously pumped (5 mL min^{-1}) by a peristaltic pump (LabV1/MC4, SHENCHEN, China) into the flow tube.[24] The Reynolds number was lower than 10 (Re = 0.2) indicating a laminar flow in the reactor.[24]

Solid phase extraction (SPE) was used on the *o*-VL liquid samples containing $NaNO_3$ and Na_2SO_4 to eliminate the salt prior to FT-ICR MS analysis. It has to be noted that during the SPE procedure, some products can be lost.[29−31] A liquid sample with volume of 3 mL was added to the SPE cartridges (Oasis WAX, 150 mg, 6 cc, 30 μm, Waters, U.S.A). The SPE cartridges were consecutively flushed by using 3 mL of acetone (3 times), methanol, and 2.5% ammonium hydroxide (NH_4OH) dissolved in methanol, respectively.[32] After activation, they were rinsed by 5 mL of Ultrapure water (18.2 MΩ cm, SARTORIUS, Germany) and dried by air stream.[32] Then, the cartridges were eluted 3 times with 3 mL of NH_4OH in methanol (2.5%).[32] Finally, the effluents were rinsed with methanol and collected in 10 mL glass vials.

2.1.1. Fourier Transform-Ion Cyclotron Resonance Mass Spectrometry (FT-ICR MS). Immediately after the SPE procedure, the liquid samples were collected and analyzed by a solariX XR FT-ICR MS instrument (Bruker Daltonik GmbH, Bremen, Germany), which comprises a refrigerated, 9.4 T actively shielded superconducting magnet (Bruker Biospin, Wissembourg, France) and a Paracell analyzer cell.[28,32] The samples were ionized by an electrospray ionization (ESI) ion source (Bruker Daltonik GmbH, Bremen, Germany) in the negative ion mode. The mass range was set to m/z 150−1000 and ion accumulation time to 0.02 s[28] A linear calibration was applied to calibrate externally the mass spectra with arginine clusters in the negative ion mode.[32] A total of 64 continuous 4 M data FT-ICR transients were coadded to increase the signal-to-noise ratio and dynamic range.[28,32] The precision of the molecular formula assignment was enhanced in such way that the final spectrum was internally recalibrated with typical O_2 class species peaks using quadratic calibration in DataAnalysis 4.4 (Bruker Daltonics).[30,32,33] A mass-resolving power ($m/\Delta m$ 50%, where Δm 50% is the mass spectral peak full width at half-maximum peak height) >450,000 was estimated at m/z 319, with <0.3 ppm absolute mass error.[28,32,33]

The most likely formulas for the detected ions were estimated by a software with a signal-to-noise ratio above 10, using a mass tolerance of ±1 ppm.[33] The maximum number of atoms was set as follows: 30 ^{12}C, 60 ^{1}H, 20 ^{16}O, 3 ^{14}N, 1 ^{32}S, 1 ^{13}C, 1 ^{18}O, and 1 ^{34}S.[33−35]

The aromaticity equivalent (X_c) has been suggested to use in order to improve the identification and characterization of aromatic and multicore aromatic compounds.[36−38] Therefore, X_c of the organic compounds, which contain C, H, O, and N in their chemical structures, was calculated as follows

$$X_c = \frac{2C + N - H - 2mO - 2nS}{DBE - mO - nS} + 1 \quad (1)$$

where m and n represent the fraction of oxygen and sulfur atoms, involved in the π-bonds of a molecular structure.[36] In our calculations, the values of m and n were set to 0.5 since the

https://doi.org/10.1021/acs.est.1c00874
Environ. Sci. Technol. 2021, 55, 4553−4564

negative mode of ESI is most sensitive to compounds that contain carboxylic functional groups.[37] Threshold values of X_c between 2.5 and 2.7 ($2.5 \leq X_c < 2.7$) and equal or greater than 2.7 ($X_c \geq 2.7$) were set as minimum criteria for the presence of aromatics or multicore aromatic compounds in the identified ions.

3. RESULTS AND DISCUSSION

3.1. Kinetic Data Treatment. The uptake coefficient (γ) of O_3 on aqueous *o*-VL, or on a mixture of *o*-VL with SO_4^{2-}, or on *o*-VL mixed with NO_3^-, was estimated as follows

$$\gamma = \frac{2rk_{1st}H_{O_3}RT}{\bar{\nu}} \quad (2)$$

where $\bar{\nu}$ = 36,000 (cm s^{-1}) at the temperature T = 296 K is the mean molecular velocity of O_3, r = 0.45 cm is the internal radius of the flow tube, k_{1st} (s^{-1}) is the first-order rate constant for the reaction between O_3 and *o*-VL ($k_{1st} = k_{2nd}$ [*o*-VL]), H_{O3} is the Henry's law coefficient of O_3 in the dilute aqueous phase ($H_{O3} = 1.13 \times 10^{-2}$ M atm^{-1}),[39] and R = 8.314 J mol K^{-1}.

Equation 2 holds when the diffusion process is not the rate-determining step.[40,41] When the reaction in the bulk aqueous phase becomes fast enough compared to the diffusion of gaseous O_3 into the liquid phase, then the reaction will not occur through the whole liquid film but solely in the upper surface layer.[42] In such a case, the heterogeneous reaction of ozone with the liquid film is controlled by the aqueous-phase diffusion process.[24,42] As a consequence, radial gas ozone concentration profiles build up from the liquid film surface to the inner glass tube walls, and the uptake coefficient of O_3 ought to be corrected to account for aqueous-phase diffusion.[24,28,40,42,43] When the uptake is controlled by diffusion, the uptake coefficient is given as follows

$$\gamma = \frac{4H_{O_3}RT\sqrt{k_{1st}D_{aq}}}{\bar{\nu}} \quad (3)$$

Considering that $k_{1st} = k_{2nd}$[o-VL], eq 3 becomes

$$\gamma = \frac{4H_{O_3}RT\sqrt{k_{2nd}[o\text{-VL}]D_{aq}}}{\bar{\nu}} \quad (4)$$

where D_{aq} is the diffusion coefficient of O_3 in the dilute aqueous phase ($D_{aq} = 1.176 \times 10^{-5}$ (cm^2 s^{-1})).[39]

According to eq 4, Figure 1 shows the dependence of the measured uptake coefficients of O_3 with the square root of the concentration of *o*-VL in the aqueous phase.

Combining eq 4 with the slope value from the linear regression of the plot depicted in Figure 1, one can estimate the second-order rate constant (k_{2nd}) for the reaction between O_3 and *o*-VL in the bulk aqueous phase. The estimated k_{2nd} = 5.4×10^5 M^{-1} s^{-1} for the aqueous-phase reaction of O_3 with *o*-VL is of the same order of magnitude as the observed second-order rate constants of O_3 with lignin-derived compounds in the bulk aqueous phase ($k_{2nd} = 2.7 \times 10^5$ M^{-1} s^{-1}).[44] However, it can be seen that the intercept of the fit of the observed uptake coefficients with eq 4 is negative. The negative intercept has no physical meaning, implying that the linear relationship is correct only for the highest concentrations of *o*-vanillin, while the equation does not describe the uptakes at lower concentrations.[43,45] This means that the bulk aqueous-phase reaction of O_3 with *o*-VL takes place together with an additional reaction involving O_3 at the liquid surface. This

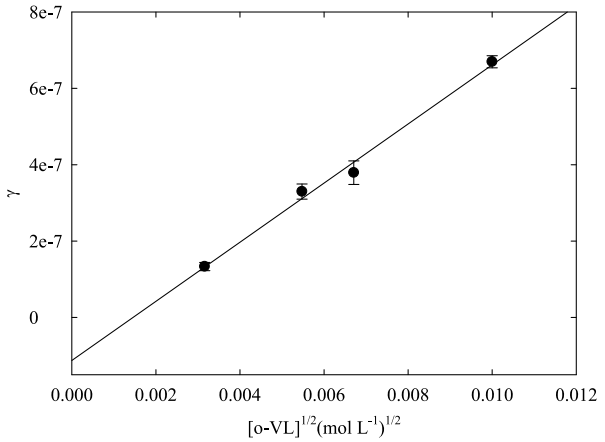

Figure 1. Uptake coefficients of O_3 (200 ppb) as a function of the square root of *o*-VL concentration in the aqueous phase. The solid line shows the fit according to eq 3.

transition between a surface-controlled regime at low concentrations of reactants and a bulk aqueous-phase regime at high reactant concentrations has been observed previously, and it can be described by the following equation[42,43,46,47]

$$\gamma = \frac{4H_{O_3}RT\sqrt{k_{2nd}[o\text{-VL}]D_{aq}}}{\bar{\nu}} + \gamma_{surf} \quad (5)$$

where γ_{surf} represents the surface reaction between O_3 and aqueous *o*-VL.

The negative intercept of the fit of the observed uptake coefficients as a function of $\sqrt{[o\text{-VL}]}$ also demonstrates that the uptakes of ozone are not controlled by liquid-phase diffusion.[42]

When Na_2SO_4 and $NaNO_3$ are added to the aqueous solution, the Henry's law coefficient of ozone ought to be adjusted by the Setchenow equation that takes into account the ionic strength effect.[24,28,48] For details about the estimation of the Henry's law coefficients of O_3 at different salt concentrations, the readers are referred to our previous studies.[24,28] The estimated Henry's law coefficients of O_3 at different Na_2SO_4 and $NaNO_3$ concentrations are reported in Table S4.

3.2. Effect of Ionic Strength on the Uptakes of O_3. Previous studies have shown that the presence of ionic strength can influence the kinetics and product distribution of reactions that take place into the aerosol deliquescent particles.[22,24,28,49−52] The presence of inorganic ions modifies the pK_a of *o*-VL, implying that it influences its protonation/deprotonation degree and, consequently, its UV-VIS absorption spectrum.[32,53] Figure S1 shows the absorbance of 1×10^{-5} mol L^{-1} *o*-VL at different ionic strengths, adjusted by Na_2SO_4. There can be observed a bathochromic shift of the n → π^* absorption band of *o*-VL, from λ_{max} = 340 nm in the dilute aqueous phase to λ_{max} = 385 nm at I = 0.9 mol L^{-1}. A similar red shift has been reported for the absorption spectra of acetosyringone (ACS) and vanillin (VL) as a function of ionic strength.[32,53] The measured pH values ranged between 8.79 and 10.11 for ionic strength values between 0.11 and 2.1 mol L^{-1} (Table S2), and the ionic-strength dependence of the uptake coefficients of O_3 due to nonadjusted pH values is shown in Figure S2. The effect of ionic strength on the uptake coefficients of ozone was investigated for an *o*-VL concentration of 1×10^{-5} M at pH 5.6. It can be seen that the uptake

https://doi.org/10.1021/acs.est.1c00874
Environ. Sci. Technol. 2021, 55, 4553−4564

coefficients of ozone (500 ppb) first increased sharply, from $(4.9 \pm 0.3) \times 10^{-7}$ at $I = 0$ to $(1.9 \pm 0.2) \times 10^{-6}$ at $I = 0.3$ mol L^{-1}, and then decreased down to $\gamma = (1.7 \pm 0.2) \times 10^{-6}$ at $I = 3$ mol L^{-1} (Figure S2).

Because the phenolic group of *o*-VL becomes ionized at higher ionic strength and pH values, the molecule tends to expand due to the electrostatic repulsion generated by the charge increment.[54] At the same time, $-O^-$ is a stronger activating group than $-OH$,[48] which leads to enhanced reactivity of *o*-VL toward ozone.

To evaluate solely the ionic strength effect on the uptake coefficients of O_3, we fixed the pH to 5.6 in both the dilute aqueous phase and in the solutions containing different ionic strengths (Na_2SO_4). The chosen conditions correspond to moderate pH values in the aerosol deliquescent particles.[55,56] Figure 2 shows the plot of log γ versus I (Na_2SO_4) at pH 5.6,

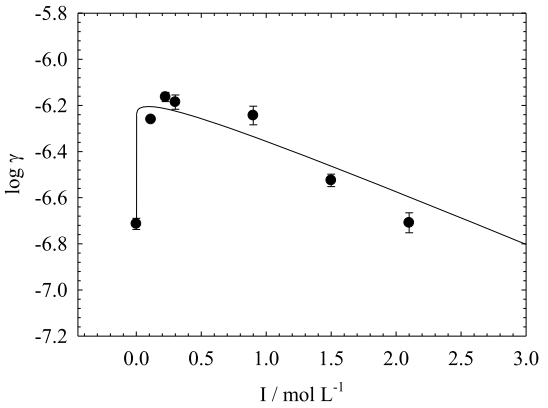

Figure 2. Uptake coefficients of gaseous ozone (200 ppb) on aqueous *o*-VL (1×10^{-5} mol L^{-1}) as a function of the molar ionic strength I (Na_2SO_4) at pH 5.6. The error bars represent 2σ.

which suggests an initial increase of the uptake coefficients of O_3 on aqueous *o*-VL, from $\gamma = (1.9 \pm 0.1) \times 10^{-7}$ at $I = 0$, to $\gamma = (6.9 \pm 0.3) \times 10^{-7}$ at $I = 0.2$ mol L^{-1} (Figure 2). At higher ionic strength, up to 2.1 mol L^{-1}, the uptakes decreased again down to $(2.0 \pm 0.1) \times 10^{-7}$. This behavior is in agreement with previous studies, focused on the ionic-strength effects on the reaction kinetics in the atmospheric aqueous phase.[30,52,57,58]

The increase of the rate constants with increasing ionic strength, up to $I \approx 0.5$ M, can be explained by the Debye–Huckel–Brønsted–Davies equation upon application of the hypothesis of Guggenheim[59−61]

$$\log k = \log k(I \to 0) + A\frac{\sqrt{I}}{1 + \sqrt{I}} + F_{ij}c_{ij} \quad (6)$$

where I is the ionic strength, A is an empirical parameter ($A = 0.51$ for water at $T = 298$ K), F_{ij} is an adjustable kinetic parameter, and c_{ij} is the concentration of Na_2SO_4.

Considering that the uptake coefficient is proportional to the square root of the measured pseudo first-order rate constants, eq 6 can be approximated as follows

$$\log \gamma = \frac{1}{2}\left(\log \gamma(I \to 0) + A\frac{\sqrt{I}}{1 + \sqrt{I}} + F_{ij}c_{ij}\right) + \frac{1}{2}\log D_{aq} - \log \frac{\bar{\nu}}{4H_{O_3}RT} \quad (7)$$

Note that γ in eq 7 is the uptake coefficient of ozone and should not be misinterpreted with activity coefficients of the reactant.[19] At low ionic strengths, a catalytic effect of the SO_4^{2-} ions leads to a sharp linear increase of the uptake coefficients, in agreement with previous studies.[52,62] The higher-order empirical term $F_{ij}c_{ij}$ in eq 7 could describe the decrease of the observed uptake coefficients at higher ionic strength values, without any physical meaning.[62]

The kinetic parameter F_{ij} emerging from the fit with eq 7 is $-(0.24 \pm 0.001)$. The obtained fit of the data predicts that the uptake coefficients would further decrease at higher ionic strength values.

The dependence of the uptake coefficients of O_3 with the ionic strength adjusted by $NaNO_3$ is shown in Figure 3.

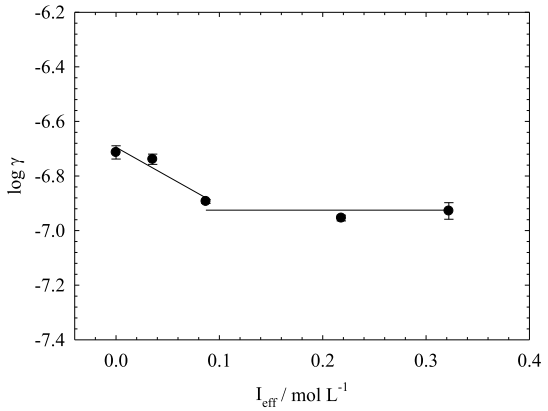

Figure 3. Uptake coefficients of gaseous ozone (200 ppb) on aqueous *o*-VL (1×10^{-5} mol L^{-1}) as a function of the effective ionic strength I_{eff} ($NaNO_3$) at pH 5.6. The error bars represent 2σ.

Note, that $NaNO_3$ is not completely dissociated in the aqueous phase. To account for this, the ionic strength values were corrected by considering the association equilibrium constant of $NaNO_3$: $K(NaNO_3/Na^+,NO_3^-) = 1.73$ M^{-1} at $T = 298$ K.[19] The effective ionic strength (I_{eff}), for a 1:1 electrolyte such as $NaNO_3$, can be estimated as follows[63]

$$I_{eff} = \sqrt{\frac{[NaNO_3]}{K} + \frac{0.25}{K^2}} - \frac{1}{2K} \quad (8)$$

When $NaNO_3$ was used as the electrolyte in aqueous solutions containing *o*-VL, the uptake coefficient of O_3 slightly decreased from $\gamma = (1.9 \pm 0.1) \times 10^{-7}$ in the absence of $NaNO_3$ to $\gamma = (1.3 \pm 0.1) \times 10^{-7}$ at $I_{eff} = 0.09$ mol L^{-1}. A further increase of the ionic strength to $I_{eff} = 0.33$ mol L^{-1} did not affect the uptake coefficients any longer (Figure 3). The linear dependence depicted in Figure 3 can be described with eq 9.[13]

$$\log k_{1st} = \log[k_{1st}(I_{eff} \to 0)] + bI_{eff} \quad (9)$$

The value of b is an empirical kinetic salting coefficient that determines the acceleration or the deceleration of the observed reaction at different ionic strengths.[19,20] The slope of the linear regression in Figure 3 gives $b = -(2.1 \pm 0.6)$ L mol^{-1} (σ-level uncertainty), which describes the deceleration of the reaction between ozone and *o*-VL. The decrease of the rate constants with ionic strength leading to a plateau was previously observed both in our laboratory[33] and by other researchers.[19]

The effect of near-UV irradiation on the relationship between the uptake coefficients of ozone and the ionic

https://doi.org/10.1021/acs.est.1c00874
Environ. Sci. Technol. 2021, 55, 4553−4564

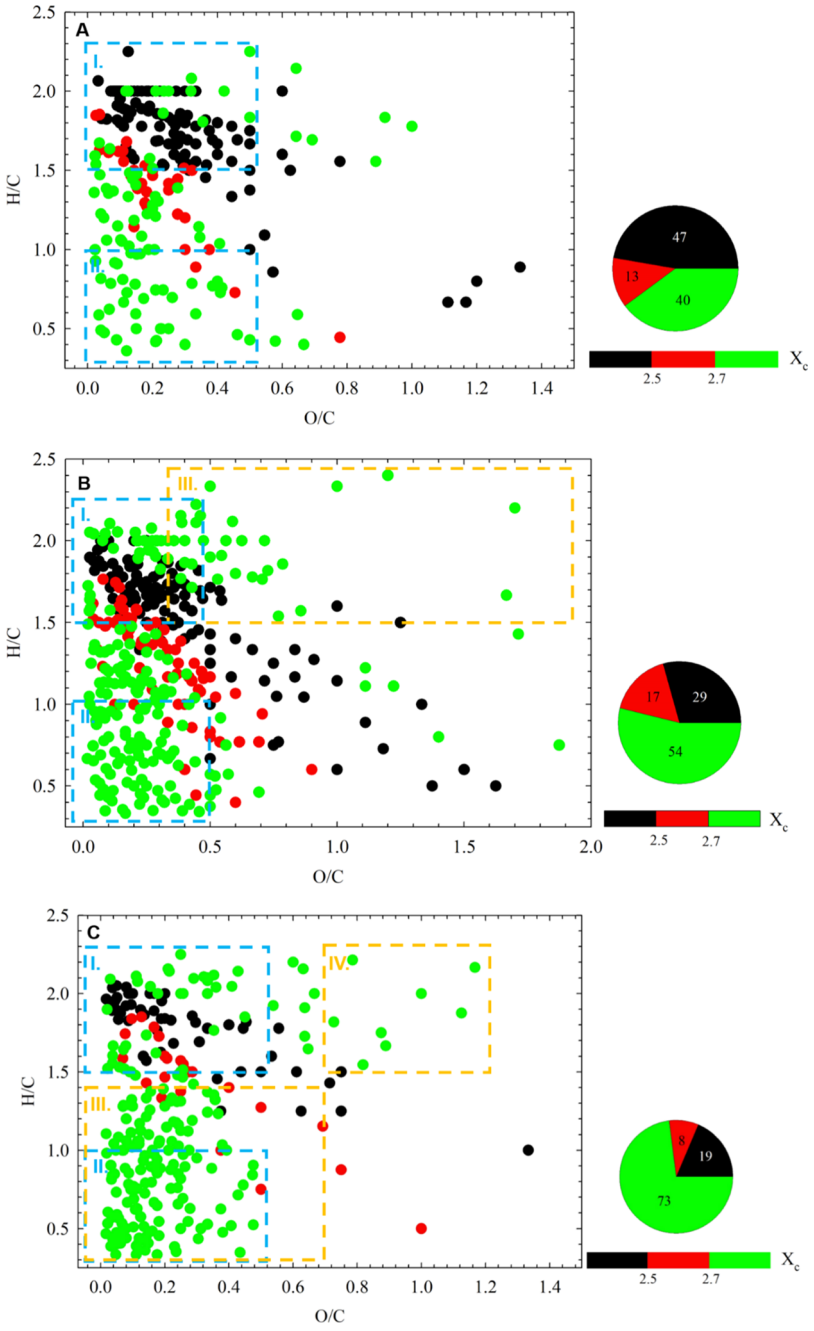

Figure 4. van Krevelen graph for the CHO, CHON, and CHOS groups of compounds, formed upon dark heterogeneous reaction of O_3 with *o*-VL (A), with a mixture of *o*-VL and SO_4^{2-} (B), and a mixture of *o*-VL and NO_3^- (C). The color coding indicates the calculated double bond equivalents (DBE) values, based on eq S1 of the Supporting Information. The aromaticity equivalent (black with $X_c < 2.5$, red with $2.5 \leq X_c < 2.7$, and green with $X_c \geq 2.7$) follows the color bar, while the pie chart shows the percentage value of each color-coded group in the sample. See the text for the description of regions I–IV.

strength was evaluated as well (Figures S3 and S4), and the results show that the O_3 uptakes are not affected by light although *o*-VL absorbs radiation in the actinic region, and its absorption spectrum overlaps with the emission spectrum of the used lamps (Figure S1). The concentration of *o*-VL used in this study was quite low (1×10^{-5} mol L^{-1}), which explains the low absorbance values reported in Figure S1. Low *o*-VL absorbance, in combination with relatively low spectral irradiance values, could account for the observed similar uptake coefficients in the dark and in the presence of light. Coherently, the liquid-phase products observed upon light-induced heterogeneous reactions of O_3 with aqueous *o*-VL did not differ from the reaction products obtained under dark conditions. For this reason, only the liquid-phase products that were observed in the dark upon heterogeneous reaction of O_3 with *o*-VL in the dilute aqueous phase and in the presence of NO_3^- and SO_4^{2-} are discussed in the section below.

3.3. Assessing the Reaction Products by FT-ICR MS. *3.3.1. CHO Class of Compounds.* In this study, 256 CHO compounds were detected in ESI^- during the heterogeneous oxidation reaction between gaseous ozone and an aqueous *o*-VL film at fixed pH 5.6. The obtained data set only provide

https://doi.org/10.1021/acs.est.1c00874
Environ. Sci. Technol. 2021, 55, 4553−4564

information on the types of the product compounds. The van Krevelen (VK) diagram, showing typical H/C versus O/C ratios, is generally used for displaying averaged compositional properties of complex organic mixtures.[64] This approach can provide a rough estimation of the different chemical characteristics of a large number of products, identified by UHR mass spectrometry.[65] The VK plot of the identified CHO compounds is illustrated in Figure 4: on the basis of H/C and O/C ratios, the identified organic products are separated into two different regions (I and II, respectively). The detected products in region I have high H/C ratio (≥1.5) and O/C ratio lower than 0.5, thereby suggesting that they are oxygenated aliphatic CHO compounds.[37,66] In contrast, compounds in region II have molecular formulas with both low H/C (≤1.0) and low O/C (≤0.5) ratios, which suggests a degree of unsaturation. For this reason, they should be monoaromatic compounds or compounds with more than one aromatic ring. Aromatic properties of the aqueous-phase CHO compounds were further examined by the use of the aromaticity equivalent (X_c) (eq 1), a mathematical parameter for the identification and characterization of aromatics with a benzene core structure ($2.50 \leq X_c < 2.71$) and of multicore aromatic compounds ($X_c \geq 2.71$). The calculation and use of X_c has been explained in detail by Yassine et al. (2014), Kourtchev et al. (2016), and Wang et al. (2017).[36−38] Based on this parameter, a large fraction of CHO compounds (47%) would have oxygenated aliphatic groups. However, still a significant fraction (40%) of products of the heterogeneous reaction of gas-phase ozone with aqueous *o*-VL are multicore aromatics, as can be seen by the position of those compounds in the lower left corner of the VK diagram.

3.3.2. Formation of Organosulfur Compounds. In this study, 399 products were detected in ESI$^-$ mode when substantial amounts of SO_4^{2-} ions (I = 2.1 M) were added to an aqueous solution of *o*-VL (pH 5.6) that was then exposed to gaseous ozone. Out of 399 identified ions, 221 were found to be CHO compounds, while 178 were assigned as CHOS compounds. Most of the CHOS products (114) possess a single sulfur atom in their molecular structure, while the others (64) have two sulfur atoms. Compared to the products of the heterogeneous reactions involving *o*-VL in the absence of any salt, the products of *o*-VL + SO_4^{2-} are clearly more numerous (see Figure 4B). More than half of the detected products of *o*-VL + SO_4^{2-} + O_3 (54%, see Figure 4B) should be multicore aromatics, as suggested by their X_c values ($X_c \geq 2.7$). The formation of compounds with more than one aromatic ring is slightly favored (increase by 14%) when I = 2.1 M (SO_4^{2-} ions), compared to the aqueous solution containing *o*-VL in the absence of any electrolytes. Coherently, these compounds show H/C < 1.0 and O/C < 0.5 (see Figure 4B, region II). However, still a significant fraction (29%) of the identified CHOS products are characterized by a high degree of saturation (H/C > 1.5) and a low degree of oxidation (O/C < 0.5) (see Figure 4B, region I). The addition of sulfate (S(VI)) ions does not favor the formation of products with a benzene-like core ($2.5 \leq X_c < 2.7$, denoted with red color coding on the VK diagram), because the formation of these aromatics is comparable with and without SO_4^{2-} ions. A 33% fraction of all the assigned CHOS molecular formulas has more than four oxygen atoms (O ≥ 4 S) and is also characterized by quite high degree of saturation (H/C > 1.5). Among all the assigned CHOS molecular formulas, 75% meet the threshold condition for being associated with organosulfates ($-OSO_3H$), and they are highlighted with the light-orange box in Figure 4B.

Table S1 comprises 61 compounds (CHO and CHOS) detected upon heterogeneous reaction of O_3 with *o*-VL in the presence of SO_4^{2-} ions, which are consistent with compounds identified in ambient aerosol samples. However, the same formulas do not imply that it is the same chemical structure as numerous structural isomers are probable for each chemical formula.[67] Nevertheless, these results suggest that the effect of ionic strength on heterogeneous ozone processing can affect the product distribution in aerosol particles.

3.3.3. Formation of Organonitrate Compounds. The heterogeneous reaction between gaseous ozone and a liquid solution at pH 5.6, containing a mixture of *o*-VL and NO_3^- (I_{eff} = 0.32 M) yielded several different classes of organic compounds, as detected in the ESI$^-$ mode. Altogether, FT-ICR MS detected 285 ions, among which 133 ions (47%) contained a single nitrogen (N) atom in their molecular structure while the others (53%) were assigned a CHO-type formula. Both identified groups of compounds covered wide mass ranges, starting from m/z 112.0 till m/z 799.0.

As shown in Figure 4C, the detected products are differentiated into four different regions (I−IV) that possess specific compositional characteristics. Compounds in boxes I and IV have a high H/C ratio (H/C > 1.5), which suggests the occurrence of highly saturated molecular structures. At the same time, the identified products in the light-blue region I possess low O/C ratio, suggesting the presence of slightly oxygenated aliphatic-like groups, which is in agreement with the low value of X_c (see black color-coding bar in Figure 4C). The compounds located in the upper right region (IV) of the VK diagram are rich in oxygen atoms and exhibit a high oxygen-to-nitrogen ratio (O/N ≥ 3), implying the formation of nitrooxy ($-ONO_2$) or oxygenated nitrooxy groups (organonitrates). The unsaturated compounds are located in the lower left part of the VK plot (regions II and III). Here, the CHON compounds that meet the criteria of O/C < 0.72 and H/C ≤ 1.36 [31] are highlighted by the light-orange box (see Figure 4C, region III) and are most probably nitroaromatics.[31,68] Compared to a dilute aqueous phase consisting of *o*-VL alone, the addition of NO_3^- ions substantially favored the formation of multicore aromatics (73%), as suggested by the X_c values (see Figure 4C, green color-coding part in the pie chart).

Table S2 comprises 22 compounds (CHO and CHON) detected upon heterogeneous reaction of O_3 with *o*-VL in the presence of NO_3^- ions, which were also identified in ambient aerosol samples collected from different locations. Through the chemical composition of all detected compounds, which was assigned by the used software (Compass DataAnalysis, Brucker), some tentatively assigned nitroaromatics with accurately detected m/z, intensity, and DBE values are listed in Table S3. Furthermore, the tentative structural properties of those nitroaromatics, which have not been detected in previous studies, are depicted in the Supporting Information.

3.3.4. Possible Formation Pathways of Organosulfates and Organonitrates. The formation of compounds containing the $-OSO_3H/-OSO_3^-$ and $-ONO_2$ groups might originate from one-electron oxidation of organic (aliphatic or aromatic) precursors by O_3. A tentative reaction scheme may be the following

$$R - H + O_3 \rightarrow R - H^+ + O_3^- \quad (R1)$$

https://doi.org/10.1021/acs.est.1c00874
Environ. Sci. Technol. 2021, 55, 4553−4564

Scheme 1. Tentative Formation Pathways that Could Account for the Formation of Some of the Detected Nitroaromatic Compounds

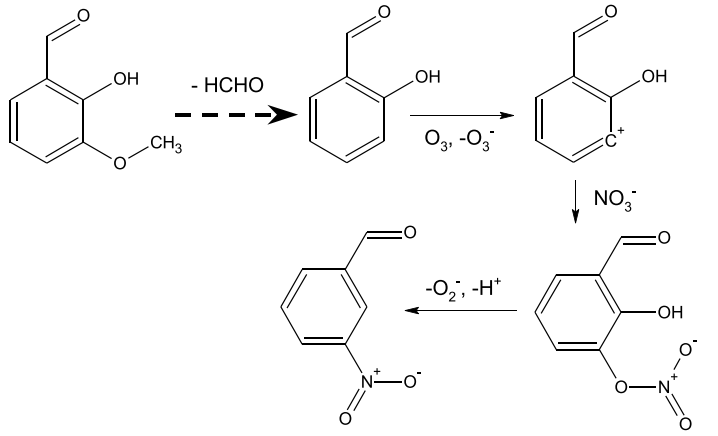

(a)

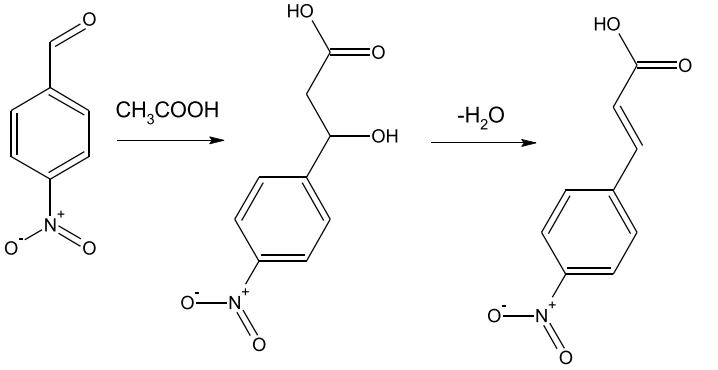

(b)

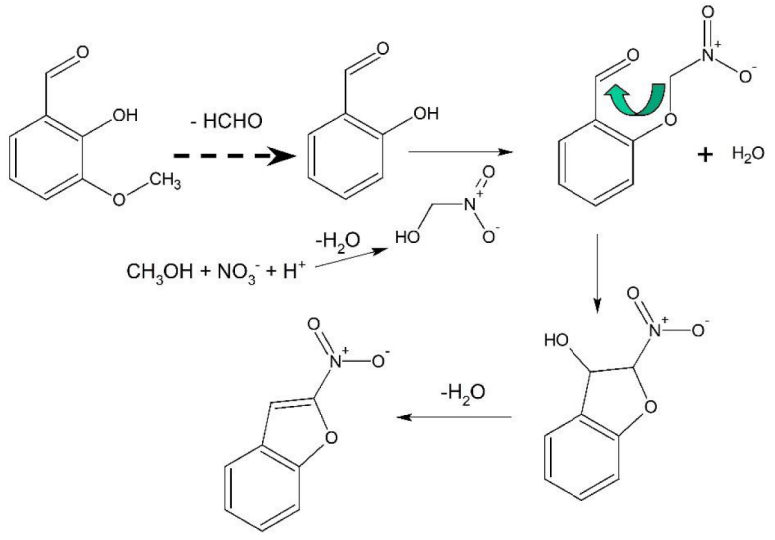

(c)

$$R - H^+ + SO_4^{2-} \rightarrow R(H)OSO_3^- \quad (R2)$$

$$R(H)OSO_3^- + O_2 \rightarrow R\text{-}OSO_3^- + HO_2^\bullet \quad (R3)$$

$$R - H^+ + NO_3^- \rightarrow R(H)ONO_2 \quad (R4)$$

$$R(H)ONO_2 + O_2 \rightarrow R - ONO_2 + HO_2^\bullet \quad (R5)$$

It is also possible to propose tentative reaction pathways to account for the formation of some nitroaromatic compounds (Scheme 1), the structures of which are reported in the Supporting Information. Nitration by nitrate ions would likely involve preoxidation by, for example, ozone,[69] while aliphatic groups might get attached to the aromatic skeleton by means of aldolic condensation. Such a process, followed by dehydration, could account for the occurrence of intermediates showing C═C double bonds.[70]

In Scheme 1, we tentatively invoke both detachment and addition of small fragments (HCHO, CH_3COOH, CH_3OH,

https://doi.org/10.1021/acs.est.1c00874
Environ. Sci. Technol. 2021, 55, 4553−4564

and its derivatives). Multiple additions of these smaller species might account for the formation of the intermediates having more complex structures (see Supporting Information for a whole list of the identified nitroaromatic compound structures).

3.3.5. Relationship between DBE and C Number. Figure 5 illustrates the distribution of the calculated DBE; (which takes into account number of π-bonds and rings in a molecule) along the molecular chains in all the identified products, as a function of the number n of C atoms. In general, the DBE values range from 1 up to 50 for n values of up to 60, and the plots follow a linear increase of the molecular masses in the presence and absence of salts. If the associated values of X_c are also considered (color code in Figure 5), it can be observed how the ozonation of *o*-VL with and without electrolytes affected the formation of homologous series with the same functional groups and similar chemical properties.

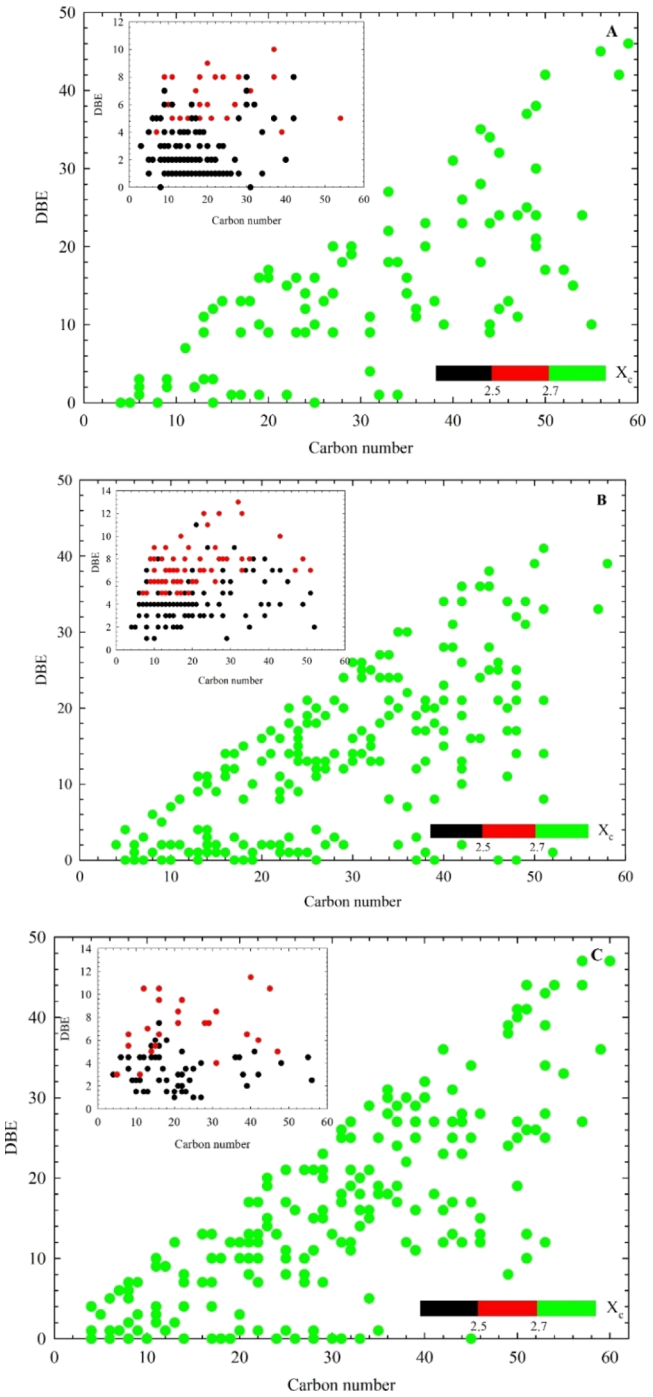

Figure 5. Iso-abundance plot of DBE vs carbon numbers for the CHO species (green circles), detected upon dark heterogeneous reaction of O_3 with aqueous *o*-VL (A), with a mixture of *o*-VL and SO_4^{2-} (B), and with a mixture of *o*-VL and NO_3^- (C). The color-coding indicates the calculated DBE values from eq S1 of the Supporting Information.

The heterogeneous ozonolysis of *o*-VL in the absence of any inorganic ions yielded long and numerous homologous series with low DBE values (DBE $\leq$ 5), which would consist of saturated, long-chain aliphatic compounds (see black color-coding peaks in Figure 5A). Several homologous series such as saturated aliphatic compounds could also be observed in the presence of SO_4^{2--} ions (black circles in Figure 5B). In contrast, the presence of NO_3^- ions reduced the formation of aliphatic compounds and produced fewer and shorter homologous series. Indeed, in analogy with previous findings, homologs were way shorter when possessing heteroatoms like S or N in their molecular structures, compared to the series composed of only CHO compounds (see black circles in Figure 5C).[71]

The presence of unsaturated compounds is suggested by relatively high DBE values (4 $\leq$ DBE $\leq$ 12) which, combined with 2.5 < X_c < 2.7, indicates the occurrence of benzene-like core structures (see red homologous series in Figure 5).

There was no significant difference in the formation of monoaromatic compounds (see red circles in Figure 5) upon heterogeneous ozonolysis of *o*-VL with or without electrolytes.

Compounds with more than one aromatic ring occurred in significant fraction upon addition of SO_4^{2-} and NO_3^- (see green circles in Figure 5B,C, respectively), when compared to the case of *o*-VL alone (Figure 5A). They feature much shorter homologous series compared to aliphatic and monoaromatic compounds, which is most likely due to their rigid molecular structure, containing mostly hydrogen and carbon atoms coupled in a series of polyaromatic-core structures. In Figure 5, the advantage of X_c classification is highlighted compared to using only DBE as an indicator of aromaticity (DBE > 7). Moreover, Figure 5 illustrates that there is a small number of the identified formulae, which using the detailed concept of X_c are regarded as polyaromatic compounds. It cannot be explained why they are characterized with X_c > 2.7, a threshold value for the presence of polyaromatics, although they do not meet the minimum requested criteria (DBE > 7 and C > 12) for polyaromatic structures (green data points in Figure 5 with DBE < 7 and C < 12).[72]

Furthermore, the formation of homologous series is additionally explored in the form of KMD vs. KM plot (Figure S5). This plot, by using a regular spacing pattern of $-CH_2$, arranges all the classified ions to make them follow the same horizontal line, if they are part of the same homologous series. The variation of DBE in those series is depicted by color coding.

These outcomes emphasize the importance of the ionic strength effect on the heterogeneous ozone reactions of methoxyphenols in the liquid core of aerosol deliquescent particles, compared to those occurring in the dilute aqueous phase of cloud droplets.

Based on the determined uptake coefficients, we estimated the atmospheric lifetime of *o*-VL as follows

https://doi.org/10.1021/acs.est.1c00874
Environ. Sci. Technol. 2021, 55, 4553−4564

$$\tau = \frac{4N_{tot}}{\gamma\bar{\nu}[O_3]_g}$$

where N_{tot} is the surface concentration of *o*-VL (molecules cm^{-2}), $\bar{\nu}$ is the mean thermal velocity of ozone (cm s^{-1}), and $[O_3]_g$ is the concentration of ozone (molecules cm^{-3}). Here, it was assumed $N_{tot} = 10^{14}$ cm^{-2}.[24,73−75] Considering an average ozone concentration (7.4×10^{14} molecules cm^{-3}), the atmospheric lifetimes of *o*-VL due to heterogeneous reaction with ozone at pH = 5.6, in a dilute aqueous phase and in the presence of 0.1 mol L^{-1} SO_4^{2-}, were calculated as 78 and 22 s, respectively. There is a competitive process between the interface reaction of OH, O_3, and also other oxidants with methoxyphenols enriched in the liquid water of aerosols. The results by Rana and Guzman (2020)[76] showed that gas-phase ozone with mixing ratios ranging between 45 and 66 ppb can break the aromatic ring of vanillin and also induce the formation of OH radicals, which in turn can react with methoxyphenols.

For comparison, the atmospheric lifetime of vanillin was estimated as 7.8 h due to reaction with OH [OH(aq)] = 7.5×10^{-15} radicals L^{-1}] on the surface of water and in aqueous particles, at pH 5.[76] The atmospheric lifetime of vanillin was estimated as 105 s due to interfacial oxidation with OH radicals ([OH]interface = $2.0\ (\pm 0.5) \times 10^{-12}$ radicals L^{-1}).[76]

Ultrahigh-resolution electrospray ionization FT-ICR MS indicates the formation of oxygenated aliphatic CHO compounds and multicore aromatics upon heterogeneous ozone processing of *o*-VL in the dilute aqueous phase. The addition of SO_4^{2-} that is typical for the liquid core of aerosol deliquescent particles increases the formation of condensed aromatics, but also organosulfates ($-OSO_3H$) arose upon ozone reactions with *o*-VL. The addition of NO_3^- ions substantially favors the formation of multicore aromatic compounds through heterogeneous ozone processing of *o*-VL. More importantly, the addition of NO_3^- ions favors the formation of organonitrates, which are potential components of the still poorly characterized light-absorbing organic matter ("brown carbon") that has the potential to affect both climate and air quality.

Considering the high ionic strength present in aerosol deliquescent particles during haze/fog events, these observations can have an important influence on the SOA formation processes through heterogeneous processing of ozone on methoxyphenols and could thus affect the radiative properties of clouds and aerosol particles.

■ ASSOCIATED CONTENT

Supporting Information

The Supporting Information is available free of charge at https://pubs.acs.org/doi/10.1021/acs.est.1c00874.

Absorption spectra of *o*-VL at different ionic strengths; uptake coefficients as a function of ionic strength; Kendrick CH_2 mass diagrams; mass spectra; variation of pH as a function of ionic strength; Henry's law coefficients of O_3 at different ionic strengths; summary of the experimental conditions; detected organic compounds; and tentatively assigned nitroaromatic compounds (PDF)

■ AUTHOR INFORMATION

Corresponding Author

Sasho Gligorovski − *State Key Laboratory of Organic Geochemistry and Guangdong Provincial Key Laboratory of Environmental Protection and Resources Utilization, Guangzhou Institute of Geochemistry, Chinese Academy of Sciences, Guangzhou 510 640, China; Guangdong-Hong Kong-Macao Joint Laboratory for Environmental Pollution and Control, Guangzhou Institute of Geochemistry and CAS Center for Excellence in Deep Earth Science, Chinese Academy of Science, Guangzhou 510640, China;* orcid.org/0000-0003-4151-2224; Phone: +86 2085291497; Email: gligorovski@gig.ac.cn

Authors

Yiqun Wang − *State Key Laboratory of Organic Geochemistry and Guangdong Provincial Key Laboratory of Environmental Protection and Resources Utilization, Guangzhou Institute of Geochemistry, Chinese Academy of Sciences, Guangzhou 510 640, China; University of Chinese Academy of Sciences, Beijing 100049, China*

Majda Mekic − *State Key Laboratory of Organic Geochemistry and Guangdong Provincial Key Laboratory of Environmental Protection and Resources Utilization, Guangzhou Institute of Geochemistry, Chinese Academy of Sciences, Guangzhou 510 640, China; University of Chinese Academy of Sciences, Beijing 100049, China;* orcid.org/0000-0001-7241-1827

Pan Li − *State Key Laboratory of Organic Geochemistry and Guangdong Provincial Key Laboratory of Environmental Protection and Resources Utilization, Guangzhou Institute of Geochemistry, Chinese Academy of Sciences, Guangzhou 510 640, China; University of Chinese Academy of Sciences, Beijing 100049, China*

Huifan Deng − *State Key Laboratory of Organic Geochemistry and Guangdong Provincial Key Laboratory of Environmental Protection and Resources Utilization, Guangzhou Institute of Geochemistry, Chinese Academy of Sciences, Guangzhou 510 640, China; University of Chinese Academy of Sciences, Beijing 100049, China*

Shiyang Liu − *State Key Laboratory of Organic Geochemistry and Guangdong Provincial Key Laboratory of Environmental Protection and Resources Utilization, Guangzhou Institute of Geochemistry, Chinese Academy of Sciences, Guangzhou 510 640, China; University of Chinese Academy of Sciences, Beijing 100049, China*

Bin Jiang − *State Key Laboratory of Organic Geochemistry and Guangdong Provincial Key Laboratory of Environmental Protection and Resources Utilization, Guangzhou Institute of Geochemistry, Chinese Academy of Sciences, Guangzhou 510 640, China;* orcid.org/0000-0002-7453-828X

Biao Jin − *State Key Laboratory of Organic Geochemistry and Guangdong Provincial Key Laboratory of Environmental Protection and Resources Utilization, Guangzhou Institute of Geochemistry, Chinese Academy of Sciences, Guangzhou 510 640, China; University of Chinese Academy of Sciences, Beijing 100049, China;* orcid.org/0000-0002-0751-7905

Davide Vione − *Dipartimento di Chimica, Università degli Studi di Torino, Torino 10125, Italy;* orcid.org/0000-0002-2841-5721

Complete contact information is available at: https://pubs.acs.org/10.1021/acs.est.1c00874

https://doi.org/10.1021/acs.est.1c00874
Environ. Sci. Technol. 2021, 55, 4553−4564

Notes

The authors declare no competing financial interest.

■ ACKNOWLEDGMENTS

This study was financially supported by the Chinese Academy of Science, International Cooperation Grant (no: 132744KYSB20190007), the National Natural Science Foundation of China (nos: 41773131, and 41977187), the State Key Laboratory of Organic Geochemistry, the Guangzhou Institute of Geochemistry (SKLOG2020-5 and KTZ_17101), and the National Key Research and Development Program (2017YFC0210103).

■ REFERENCES

(1) Simpson, C. D.; Paulsen, M.; Dills, R. L.; Liu, L.-J. S.; Kalman, D. A. Determination of Methoxyphenols in Ambient Atmospheric Particulate Matter: Tracers for Wood Combustion. *Environ. Sci. Technol.* **2005**, *39*, 631−637.

(2) Mazzoleni, L. R.; Zielinska, B.; Moosmüller, H. Emissions of Levoglucosan, Methoxy Phenols, and Organic Acids from Prescribed Burns, Laboratory Combustion of Wildland Fuels, and Residential Wood Combustion. *Environ. Sci. Technol.* **2007**, *41*, 2115−2122.

(3) Vione, D.; Maurino, V.; Minero, C.; Pelizzetti, E.; Harrison, M. A. J.; Olariu, R.-I.; Arsene, C. Photochemical reaction in the tropospheric aqueous phase and on matriculate matter. *Chem. Soc. Rev.* **2006**, *35*, 441−453.

(4) Hawthorne, S. B.; Krieger, M. S.; Miller, D. J.; Mathiason, M. B. Collection and Quantitation of Methoxylated Phenol Tracers for Atmospheric Pollution from Residential Wood Stoves. *Environ. Sci. Technol.* **1989**, *23*, 470−475.

(5) Schauer, J. J.; Kleeman, M. J.; Cass, G. R.; Simoneit, B. R. T. Measurement of Emissions from Air Pollution Sources. 3. C1−C29Organic Compounds from Fireplace Combustion of Wood. *Environ. Sci. Technol.* **2001**, *35*, 1716−1728.

(6) Simoneit, B. R. T. Biomass burning - a review of organic tracers for smoke from incomplete combustion. *Appl. Geochem.* **2002**, *17*, 129−162.

(7) Sander, R. Compilation of Henry's law constants (version 4.0) for water as solvent. *Atmos. Chem. Phys.* **2015**, *15*, 4399−4981.

(8) Yee, L. D.; Kautzman, K. E.; Loza, C. L.; Schilling, K. A.; Coggon, M. M.; Chhabra, P. S.; Chan, M. N.; Chan, A. W. H.; Hersey, S. P.; Crounse, J. D.; Wennberg, P. O.; Flagan, R. C.; Seinfeld, J. H. Secondary organic aerosol formation from biomass burning intermediates: phenol and methoxyphenols. *Atmos. Chem. Phys.* **2013**, *13*, 8019−8043.

(9) Lauraguais, A.; Coeur-Tourneur, C.; Cassez, A.; Deboudt, K.; Fourmentin, M.; Choël, M. Atmospheric reactivity of hydroxyl radicals with guaiacol (2-methoxyphenol), a biomass burning emitted compound: Secondary organic aerosol formation and gas-phase oxidation products. *Atmos. Environ.* **2014**, *86*, 155−163.

(10) Liu, C.; Liu, J.; Liu, Y.; Chen, T.; He, H. Secondary organic aerosol formation from the OH-initiated oxidation of guaiacol under different experimental conditions. *Atmos. Environ.* **2019**, *207*, 30−37.

(11) Net, S.; Nieto-Gligorovski, L.; Gligorovski, S.; Wortham, H. Heterogeneous ozonation kinetics of 4-phenoxyphenol in the presence of photosensitizer. *Atmos. Chem. Phys.* **2010**, *10*, 1545−1554.

(12) Net, S.; Gligorovski, S.; Pietri, S.; Wortham, H. Photoenhanced degradation of veratraldehyde upon the heterogeneous ozone reactions. *Phys. Chem. Chem. Phys.* **2010**, *12*, 7603−7611.

(13) Zein, A. E.; Coeur, C.; Obeid, E.; Lauraguais, A.; Fagniez, T. Reaction Kinetics of Catechol (1,2-Benzenediol) and Guaiacol (2-Methoxyphenol) with Ozone. *J. Phys. Chem. A* **2015**, *119*, 6759−6765.

(14) Sun, Y.; Xu, F.; Li, X.; Zhang, Q.; Gu, Y. Mechanisms and kinetic studies of OH-initiated atmospheric oxidation of methoxyphenols in the presence of O2 and NOx. *Phys. Chem. Chem. Phys.* **2019**, *21*, 21856−21866.

(15) Jammoul, A.; Gligorovski, S.; George, C.; D'Anna, B. Photosensitized Heterogeneous Chemistry of Ozone on Organic Films. *J. Phys. Chem. A* **2008**, *112*, 1268−1276.

(16) Zhang, T.; Yang, W.; Han, C.; Yang, H.; Xue, X. Heterogeneous reaction of ozone with syringic acid: Uptake of O3 and changes in the composition and optical property of syringic acid. *Environ. Pollut.* **2020**, *257*, 113632.

(17) He, L.; Schaefer, T.; Otto, T.; Kroflič, A.; Herrmann, H. Kinetic and Theoretical Study of the Atmospheric Aqueous-Phase Reactions of OH Radicals with Methoxyphenolic Compounds. *J. Phys. Chem. A* **2019**, *123*, 7828−7838.

(18) Pang, H.; Zhang, Q.; Lu, X.; Li, K.; Chen, H.; Chen, J.; Yang, X.; Ma, Y.; Ma, J.; Huang, C. Nitrite-Mediated Photooxidation of Vanillin in the Atmospheric Aqueous Phase. *Environ. Sci. Technol.* **2019**, *53*, 14253−14263.

(19) Herrmann, H. Kinetics of Aqueous Phase Reactions Relevant for Atmospheric Chemistry. *Chem. Rev.* **2003**, *103*, 4691−4716.

(20) Herrmann, H.; Schaefer, T.; Tilgner, A.; Styler, S. A.; Weller, C.; Teich, M.; Otto, T. Tropospheric Aqueous-Phase Chemistry: Kinetics, Mechanisms, and Its Coupling to a Changing Gas Phase. *Chem. Rev.* **2015**, *115*, 4259−4334.

(21) Cheng, Y.; Zheng, G.; Wei, C.; Mu, Q.; Zheng, B.; Wang, Z.; Gao, M.; Zhang, Q.; He, K.; Carmichael, G.; Pöschl, U.; Su, H. Reactive nitrogen chemistry in aerosol water as a source of sulfate during haze events in China. *Sci. Adv.* **2016**, *2*, No. e1601530.

(22) Mekic, M.; Gligorovski, S. Ionic strength effects on heterogeneous and multiphase chemistry: Clouds versus aerosol particles. *Atmos. Environ.* **2021**, *244*, 117911.

(23) Huang, D. D.; Zhang, Q.; Cheung, H. H. Y.; Yu, L.; Zhou, S.; Anastasio, C.; Smith, J. D.; Chan, C. K. Formation and evolution of aqSOA from aqueous-phase reactions of phenolic carbonyls: comparison between ammonium sulfate and ammonium nitrate solutions. *Environ. Sci. Technol.* **2018**, *52*, 9215−9224.

(24) Mekic, M.; Wang, Y.; Loisel, G.; Vione, D.; Gligorovski, S. Ionic strength effect alters the heterogeneous ozone oxidation of methoxyphenols in going from cloud droplets to aerosol deliquescent particles. *Environ. Sci. Technol.* **2020**, *54*, 12898−12907.

(25) Shi, G.; Xu, J.; Peng, X.; Xiao, Z.; Chen, K.; Tian, Y.; Guan, X.; Feng, Y.; Yu, H.; Nenes, A.; Russell, A. G. pH of Aerosols in a Polluted Atmosphere: Source Contributions to Highly Acidic Aerosol. *Environ. Sci. Technol.* **2017**, *51*, 4289−4296.

(26) Wang, G.; Zhang, F.; Peng, J.; Duan, L.; Ji, Y.; Marrero-Ortiz, W.; Wang, J.; Li, J.; Wu, C.; Cao, C.; Wang, Y.; Zheng, J.; Secrest, J.; Li, Y.; Wang, Y.; Li, H.; Li, N.; Zhang, R. Particle acidity and sulfate production during severe haze events in China cannot be reliably inferred by assuming a mixture of inorganic salts. *Atmos. Chem. Phys.* **2018**, *18*, 10123−10132.

(27) Wang, J.; Li, J.; Ye, J.; Zhao, J.; Wu, Y.; Hu, J.; Liu, D.; Nie, D.; Shen, F.; Huang, X.; Huang, D.; Ji, D.; Sun, X.; Xu, W.; Guo, J.; Song, S.; Qin, Y.; Liu, P.; Turner, J. R.; Lee, H. C.; Hwang, S.; Liao, H.; Martin, S. T.; Zhang, Q.; Chen, M.; Sun, Y.; Ge, X.; Jacob, D. J. Fast sulfate formation from oxidation of SO2 by NO2 and HONO observed in Beijing haze. *Nat. Commun.* **2020**, *11*, 2844−2851.

(28) Mekic, M.; Loisel, G.; Zhou, W.; Jiang, B.; Vione, D.; Gligorovski, S. Ionic-Strength Effects on the Reactive Uptake of Ozone on Aqueous Pyruvic Acid: Implications for Air-Sea Ozone Deposition. *Environ. Sci. Technol.* **2018**, *52*, 12306−12315.

(29) LeClair, J. P.; Collett, J. L.; Mazzoleni, L. R. Fragmentation Analysis of Water-Soluble Atmospheric Organic Matter Using Ultrahigh-Resolution FT-ICR Mass Spectrometry. *Environ. Sci. Technol.* **2012**, *46*, 4312−4322.

(30) Zhao, Y.; Hallar, A. G.; Mazzoleni, L. R. Atmospheric organic matter in clouds: exact masses and molecular formula identification using ultrahigh-resolution FT-ICR mass spectrometry. *Atmos. Chem. Phys.* **2013**, *13*, 12343−12362.

(31) Bianco, A.; Riva, M.; Baray, J.-L.; Ribeiro, M.; Chaumerliac, N.; George, C.; Bridoux, M.; Deguillaume, L. Chemical Characterization of Cloudwater Collected at Puy de Dôme by FT-ICR MS Reveals the

https://doi.org/10.1021/acs.est.1c00874
Environ. Sci. Technol. 2021, 55, 4553−4564

Presence of SOA Components. *ACS Earth Space Chem.* **2019**, *3*, 2076−2087.
(32) Loisel, G.; Mekic, M.; Liu, S.; Song, W.; Jiang, B.; Wang, Y.; Deng, H.; Gligorovski, S. Ionic strength effect on the formation of organonitrate compounds through photochemical degradation of vanillin in liquid water of aerosols. *Atmos. Environ.* **2021**, *246*, 118140.
(33) Vione, D.; Albinet, A.; Barsotti, F.; Mekic, M.; Jiang, B.; Minero, C.; Brigante, M.; Gligorovski, S. Formation of substances with humic-like fluorescence properties, upon photoinduced oligomerization of typical phenolic compounds emitted by biomass burning. *Atmos. Environ.* **2019**, *206*, 197−207.
(34) Shi, Q.; Pan, N.; Long, H.; Cui, D.; Guo, X.; Long, Y.; Chung, K. H.; Zhao, S.; Xu, C.; Hsu, C. S. Characterization of middle-temperature gasification coal tar. Part 3: Molecular composition of acidic compounds. *Energy Fuels* **2013**, *27*, 108−117.
(35) Jiang, B.; Liang, Y.; Xu, C.; Zhang, J.; Hu, M.; Shi, Q. Polycyclic Aromatic Hydrocarbons (PAHs) in Ambient Aerosols from Beijing: Characterization of Low Volatile PAHs by Positive-Ion Atmospheric Pressure Photoionization (APPI) Coupled with Fourier Transform Ion Cyclotron Resonance. *Environ. Sci. Technol.* **2014**, *48*, 4716−4723.
(36) Yassine, M. M.; Harir, M.; Dabek-Zlotorzynska, E.; Schmitt-Kopplin, P. Structural characterization of organic aerosol using Fourier transform ion cyclotron resonance mass spectrometry: Aromaticity equivalent approach. *Rapid Commun. Mass Spectrom.* **2014**, *28*, 2445−2454.
(37) Kourtchev, I.; Godoi, R. H. M.; Connors, S.; Levine, J. G.; Archibald, A. T.; Godoi, A. F. L.; Paralovo, S. L.; Barbosa, C. G. G.; Souza, R. A. F.; Manzi, A. O.; Seco, R.; Sjostedt, S.; Park, J.-H.; Guenther, A.; Kim, S.; Smith, J.; Martin, S. T.; Kalberer, M. Molecular composition of organic aerosols in central Amazonia: an ultra-high-resolution mass spectrometry study. *Atmos. Chem. Phys.* **2016**, *16*, 11899−11913.
(38) Wang, X. K.; Hayeck, N.; Brüggemann, M.; Yao, L.; Chen, H.; Zhang, C.; Emmelin, C.; Chen, J.; George, C.; Wang, L. Chemical Characterization of Organic Aerosols in Shanghai: A Study by Ultra-High-Performance Liquid Chromatography Coupled With Orbitrap Mass Spectrometry. *J. Geophys. Res. Atmos.* **2017**, *122*, 11703−11722.
(39) Johnson, P. N.; Davis, R. A. Diffusivity of ozone in water. *J. Chem. Eng. Data* **1996**, *41*, 1485−1487.
(40) Behnke, W.; George, C.; Scheer, V.; Zetzsch, C. Production and decay of ClNO2from the reaction of gaseous N2O5with NaCl solution: Bulk and aerosol experiments. *J. Geophys. Res.* **1997**, *102*, 3795−3804.
(41) Barcellos da Rosa, M.; Behnke, W.; Zetzsch, C. Study of the heterogeneous reaction of O3 with CH3SCH3 using the wetted-wall flowtube technique. *Atmos. Chem. Phys.* **2003**, *3*, 1665−1673.
(42) Gutzwiller, L.; George, C.; Rössler, E.; Ammann, M. Reaction Kinetics of NO2with Resorcinol and 2,7-Naphthalenediol in the Aqueous Phase at Different pH. *J. Phys. Chem. A* **2002**, *106*, 12045−12050.
(43) Clifford, D.; Donaldson, D. J.; Brigante, M.; D'Anna, B.; George, C. Reactive Uptake of Ozone by Chlorophyll at Aqueous Surfaces. *Environ. Sci. Technol.* **2008**, *42*, 1138−1143.
(44) Khudoshin, A. G.; Mitrofanova, A. N.; Lunin, V. V. Lignin Transformations and Reactivity upon Ozonation in Aqueous Media. *Russ. J. Phys. Chem.* **2012**, *86*, 360−365.
(45) Brigante, M.; D'Anna, B.; Conchon, P.; George, C. Multiphase Chemistry of Ozone on Fulvic Acids Solutions. *Environ. Sci. Technol.* **2008**, *42*, 9165−9170.
(46) Hu, J. H.; Shi, Q.; Davidovits, P.; Worsnop, D. R.; Zahniser, M. S.; Kolb, C. E. Reactive Uptake of Cl2(g) and Br2(g) by Aqueous Surfaces as a Function of Br- and I- Ion Concentration: The Effect of Chemical Reaction at the Interface. *J. Phys. Chem.* **1995**, *99*, 8768−8776.
(47) George, C.; Behnke, W.; Scheer, V.; Zetzsch, C.; Magi, L.; Ponche, J. L.; Mirabel, P. Fate of ClNO2over aqueous solutions containing iodide. *Geophys. Res. Lett.* **1995**, *22*, 1505−1508.
(48) Beltran, F. J. *Ozone Reaction Kinetics for Water and Wastewater Systems*; CRC Press LLC: Boca Raton, FL, 2004.
(49) Mekic, M.; Brigante, M.; Vione, D.; Gligorovski, S. Exploring the ionic strength effects on the photochemical degradation of pyruvic acid in atmospheric deliquescent aerosol particles. *Atmos. Environ.* **2018**, *185*, 237−242.
(50) Oldridge, N. W.; Abbatt, J. P. D. Formation of Gas-Phase Bromine from Interaction of Ozone with Frozen and Liquid NaCl/NaBr Solutions: Quantitative Separation of Surficial Chemistry from Bulk-Phase Reaction. *J. Phys. Chem. A* **2011**, *115*, 2590−2598.
(51) Reeser, D. I.; Jammoul, A.; Clifford, D.; Brigante, M.; D'Anna, B.; George, C.; Donaldson, D. J. Photoenhanced Reaction of Ozone with Chlorophyll at the Seawater Surface. *J. Phys. Chem. C* **2009**, *113*, 2071−2077.
(52) Mekic, M.; Zeng, J.; Zhou, W.; Loisel, G.; Jin, B.; Li, X.; Vione, D.; Gligorovski, S. Ionic Strength Effect on Photochemistry of Fluorene and Dimethylsulfoxide at the Air-Sea Interface: Alternative Formation Pathway of Organic Sulfur Compounds in a Marine Atmosphere. *ACS Earth Space Chem.* **2020**, *4*, 1029−1038.
(53) Zhou, W.; Mekic, M.; Liu, J.; Loisel, G.; Jin, B.; Vione, D.; Gligorovski, S. Ionic strength effects on the photochemical degradation of acetosyringone in atmospheric deliquescent aerosol particles. *Atmos. Environ.* **2019**, *198*, 83−88.
(54) Alvarez-Puebla, R. A.; Valenzuela-Calahorro, C.; Garrido, J. J. Theoretical study on fulvic acid structure, conformation and aggregation. *Sci. Total Environ.* **2006**, *358*, 243−254.
(55) Guo, H.; Xu, L.; Bougiatioti, A.; Cerully, K. M.; Capps, S. L.; Hite, J. R., Jr.; Carlton, A. G.; Bergin, M. H.; Ng, N. L.; Nenes, A.; Weber, R. J.; Weber, R. J. Fine-particle water and pH in the southeastern United States. *Atmos. Chem. Phys.* **2015**, *15*, 5211−5228.
(56) Pye, H. O. T.; Nenes, A.; Alexander, B.; Ault, A. P.; Barth, M. C.; Clegg, S. L.; Collett, J. L., Jr.; Fahey, K. M.; Hennigan, C. J.; Herrmann, H.; Kanakidou, M.; Kelly, J. T.; Ku, I.-T.; McNeill, V. F.; Riemer, N.; Schaefer, T.; Shi, G.; Tilgner, A.; Walker, J. T.; Wang, T.; Weber, R.; Xing, J.; Zaveri, R. A.; Zuend, A. The acidity of atmospheric particles and clouds. *Atmos. Chem. Phys.* **2020**, *20*, 4809−4888.
(57) Clarke, A. G.; Radojevic, M. Chloride ion effects on the aqueous oxidation of So2. *Atmos. Environ.* **1983**, *17*, 617.
(58) Lagrange, J.; Pallares, C.; Wenger, G.; Lagrange, P. Electrolyte Effects on Aqueous Atmospheric Oxidation of Sulphur Dioxide by Hydrogen Peroxide. *Atmos. Environ.* **1993**, *27*, 129−137.
(59) Liu, Y.; Sheaffer, R. L.; Barker, J. R. Effects of Temperature and Ionic Strength on the Rate and Equilibrium Constants for the Reaction Iaq+ I-aq↔ I2-aq. *J. Phys. Chem. A* **2003**, *107*, 10296−10302.
(60) Guggenheim, E. A.; Wiseman, L. A. Kinetic Salt Effects on the Inversion of Sucrose. *Proc. Roy. Soc. Lond. Math. Phys. Sci.* **1950**, *203*, 17−32.
(61) Perlmutter-Hayman, B.; Stein, G. Specific Ionic Effects on Reaction Rates. The Reaction between Persulfate and Iodide Ions in the Presence of High Concentrations of Added Salts. *J. Chem. Phys.* **1964**, *40*, 848−852.
(62) Bao, Z.-C.; Barker, J. R. Temperature and Ionic Strength Effects on Some Reactions Involving Sulfate Radical [SO4-(aq)]. *J. Phys. Chem.* **1996**, *100*, 9780−9787.
(63) von Bünau, G.; Wolff, T. *Photochemie, Grundlagen, Methoden, Anwendungen*; VCH Verlagsgesellschaft, Wiley-VCH: Weinheim, Germany, 1987.
(64) van Krevelen, D. W. *Coal: Typology—Chemistry—Physics—Constitution*, 3rd ed.; Elsevier: New York, 1993.
(65) Jiang, B.; Kuang, B. Y.; Liang, Y.; Zhang, J.; Huang, X. H. H.; Xu, C.; Yu, J. Z.; Shi, Q. Molecular composition of urban organic aerosols on clear and hazy days in Beijing: a comparative study using FT-ICR MS. *Environ. Chem.* **2016**, *13*, 888−901.
(66) Wang, K.; Zhang, Y.; Huang, R.-J.; Cao, J.; Hoffmann, T. UHPLC-Orbitrap mass spectrometric characterization of organic aerosol from a central European city (Mainz, Germany) and a Chinese megacity (Beijing). *Atmos. Environ.* **2018**, *189*, 22−29.

https://doi.org/10.1021/acs.est.1c00874
Environ. Sci. Technol. 2021, 55, 4553−4564

(67) Nizkorodov, S. A.; Laskin, J.; Laskin, A. Molecular chemistry of organic aerosols through the application of high resolution mass spectrometry. *Phys. Chem. Chem. Phys.* **2011**, *13*, 3612−3629.
(68) Altieri, K. E.; Turpin, B. J.; Seitzinger, S. P. Composition of Dissolved Organic Nitrogen in Continental Precipitation Investigated by Ultra-High Resolution FT-ICR Mass Spectrometry. *Environ. Sci. Technol.* **2009**, *43*, 6950−6955.
(69) von Sonntag, C.; von Gunten, U. *Chemistry of Ozone in Water and Wastewater Treatment, From Basic Principles to Applications*; IWA Publishing: London, U.K., 2012; p 320.
(70) Smith, M. B. *March's Advanced Organic Chemistry: Reactions, Mechanisms, and Structure*, 7th ed.; Wiley: NY, 2013; p 2080.
(71) Rincón, A. G.; Calvo, A. I.; Dietzel, M.; Kalberer, M. Seasonal differences of urban organic aerosol composition - an ultra-high resolution mass spectrometry study. *Environ. Chem.* **2012**, *9*, 298−319.
(72) Tong, H.; Kourtchev, I.; Pant, P.; Keyte, I. J.; O'Connor, I. P.; Pope, F. D.; Harrison, R. M.; Kalberer, M.; Kalberer, M. Molecular composition of organic aerosols at urban background and road tunnel sites using ultra-high resolution mass spectrometry. *Faraday Discuss.* **2016**, *189*, 51−68.
(73) Knopf, D. A.; Forrester, S. M.; Slade, J. H. Heterogeneous oxidation kinetics of organic biomass burning aerosol surrogates by O3, NO2, N2O5, and NO3. *Phys. Chem. Chem. Phys.* **2011**, *13*, 21050−21062.
(74) Gross, S.; Bertram, A. K. Reactive Uptake of NO3, N2O5, NO2, HNO3, and O3on Three Types of Polycyclic Aromatic Hydrocarbon Surfaces. *J. Phys. Chem. A* **2008**, *112*, 3104−3113.
(75) Moise, T.; Rudich, Y. Uptake of Cl and Br by organic surfaces-A perspective on organic aerosols processing by tropospheric oxidants. *Geophys. Res. Lett.* **2001**, *28*, 4083−4086.
(76) Rana, M. S.; Guzman, M. I. Oxidation of Phenolic Aldehydes by Ozone and Hydroxyl Radicals at the Air-Water Interface. *J. Phys. Chem. A* **2020**, *124*, 8822−8833.

https://doi.org/10.1021/acs.est.1c00874
Environ. Sci. Technol. 2021, 55, 4553−4564